Supporting Information

The ultrafast reconfigurability and ultrahigh durability of NiFe phosphides electrocatalyst with a Fe-rich surface induced by in-situ acid corrosion for water oxidations

Min Jiang,[a] Jiaming Zhang, [b] Hanxiao Liao, [a] Huanhuan Zhai, [a] Xuanzhi Liu, [a] Pengfei Tan[*a], Ke Yang*[*c] and Jun Pan*[*a]*

[a]State Key Laboratory for Powder Metallurgy, Central South University Lushan South Street 932, Changsha 410083, China.

[b]School of Chemistry and Chemical Engineering, Central South University Lushan South Street 932, Changsha 410083, China.

[c]Department of Applied Physics, The Hong Kong Polytechnic University, Kowloon, Hong Kong, China.

*corresponding author: jun.pan@csu.edu.cn; keyanghnu@gmail.com; tpf0203@csu.edu.cn

Fax: +86-731-88871017; Tel: +86-731-88836329

Experimental Section

Chemicals and materials: Nickel iron foam (NFF; thickness: 1.5 mm; number of pores per inch: 95 ppi; atomic ratio of Ni/Fe = 1:1), nickel foam (NF, 1.5 mm, 95 ppi), iron foam (FF, 1.5 mm, 95 ppi), were purchased from Kunshan Longshengbao Electronic Material Co., Ltd. (Note: The commercial NFF is heterogeneous but repeatable.) Potassium hydroxide (KOH, AR, 98%) and hydrochloric acid (HCl, AR, 36%) were purchased from Sinopharm Chemical Reagent Co., Ltd. Red phosphorous (P, AR, 98.5%) were purchased from Aladdin Chemistry Co., Ltd.

Synthesis of o-NiFe foam: Prior to synthesis, 1×1.5 cm^2 of commercial NiFe foam was washed with 1.0 M HCl solutions for 10 min, then rinsed with ultrapure water and dried with a hair dryer. Subsequently, the cleaned NiFe foam was immersed in a beaker containing 10 mM HCl solutions. After stirring and sonication for 5 min, the moist NiFe foam was removed and allowed to stand in air for 1 h. After rinsing with ultrapure water and drying with a hair dryer, o-NiFe foam was obtained.

Synthesis of o-NiFeP/NFF, o-NiP/NF, and o-FeP/FF: Red phosphorus (50 mg) and four pieces of o-NiFe foam (1×1.5 cm^2) were placed upstream (inlet) and downstream of the tube furnace. Subsequently, the samples were heated to 500 °C (10 °C/min) under a nitrogen atmosphere and held for 1 h. After cooling, the o-NiFeP/NFF pre-catalyst was obtained.

As comparison samples, o-NiP/NF and o-FeP/FF were prepared in the same way as o-NiFeP/NFF, except that Ni foam (NF) and Fe Foam (FF) were used as substrate materials, respectively.

Synthesis of NiFeP/NFF: NiFeP/NFF is prepared in a similar way to o-NiFeP/NFF, except that the NiFe foam without acid etching is directly used for phosphating treatment.

Characterizations: The morphologies and element contents were detected via double beam scanning electron microscope systems (SEM, Helios Nanolab G3 UC), which equipped with an Energy Dispersive X-ray detector (EDS, Team Octane Plus), as well as Inductively coupled plasma mass spectrometry (ICP-MS, Agilent 720ES). X-ray diffraction (XRD) and Transmission electron microscopy (TEM) characterizations

were carried out on a Rigaku-TTRIII and a TecnaiG2 20ST, respectively. All XPS spectra were obtained on X-ray photoelectron spectrometer (XPS, K-Alpha 1063) and corrected using C1s line at 284.8 eV. Raman measurements were performed on a micro-Raman spectrometer (DXR3) under an excitation of 532 nm laser light.

Electrochemical measurements: All the OER catalytic measurements were carried out on a CHI660E electrochemistry workstation in 1.0 M KOH electrolyte with a typical three-electrode system, in which the as-prepared electrocatalyst with geometric area of 1×1 cm^2 soaked into electrolyte as the working electrode, a Pt sheet as the counter electrode, and an Ag/AgCl electrode as the reference electrode. Then the RHE potentials in the three electrolytes were determined from the corresponding open-circuit potentials (-1.015 V for 1.0 M KOH). The electrode potential was converted to the RHE scale using E (vs. RHE) = E (vs. Ag/AgCl) + 1.015 V for the measurements in 1.0 M KOH electrolyte. The overpotential (η) was calculated by η = E (vs. RHE) -1.23 V for OER.

200 cyclic voltammetry (CV) scans (50 mV s^{-1}, 0-0.8 V vs. Ag/AgCl) were applied to remove the surface contaminants and electrochemically activate the catalysts to achieve a relatively stable performance before linear sweep voltammetry (LSV) measurements. LSV was recorded at a scan rate of 5 mV s^{-1} with *i*R-correction (90%). 200 CV scans (50 mV s^{-1}, 0-0.1 V vs. Ag/AgCl) were applied before investigating surface reconstruction affected by CV activation in OER. Cyclic voltammetry (CV) tested at different scan rates for obtaining electrochemical double layer capacitance (Cdl) values; Electrochemical impedance spectroscopy (EIS) tests were carried out from 100 kHz to 10 mHz.

The Tafel slope was calculated by the equation below:

$$\eta = a + blog(j)$$

Where η stands for the overpotential, b stands for the Tafel slope, j stands for the current density.

First-principles calculations

The spin-polarized Density functional theory (DFT) calculations were performed to study catalytic mechanism in VASP[1, 2] with a projector augmented wave (PAW) basis[3]. The Perdew-Burke-Ernzerhof (PBE) Generalized Gradient Approximation (GGA) exchange-correlation functional method was used to describe the exchange-correlation interaction. For all the calculations, the kinetic energy cutoff for electronic plane wave expansion was set to 450 eV. Brillouin zone integration was performed on grids *Γ*-centered 3×3×1 k-points-grids for the structural relaxation and electronic structure calculations. The DFT/GGA+U were performed (Fe 3d and Ni 3d were 4 and 3 eV) to consider to strong correction interaction[4]. Moreover, the dispersive van der Waals (vdW) interactions were also taken into account by the zero damping DFT-D3 method with Becke-Jonson damping[5, 6]. Total energy and the forces on each atom were converged to less than 10^{-6} eV and 0.03 eV/Å, respectively. The vacuum layer of around 15 Å along z direction was inserted to eliminate the spurious interaction between periodic images. The Gibbs free energy change was calculated[7, 8]:

$$\Delta G = \Delta E + \Delta E_{ZPE} - T\Delta S + \Delta G_{pH} + \Delta G_V$$

where ΔE is the reaction energy. ΔE_{ZPE} and ΔS are the change in the zero-point energy and the vibrational entropy at temperature *T*, respectively. $\Delta G_{pH} = k_B T \times pH \times \ln 10$ is the correction from the proton concentration as indicated by the pH value, where k_B is the Boltzmann constant. $\Delta G_V = eV$ is the correction from the applied electrode potential (*V*). Here, the standard conditions were adopted, *i.e.,* pressure $p = 1$ bar, $pH = 14$ and $T = 298.15$ K. The (0001) surface of $Ni_{2-x}Fe_xP$ (x=0~0.33) and $(01\bar{1}2)$ surface of NiFeOOH with Fe-rich and Ni-rich have been select to study the catalytic properties, as shown in Figure S4.

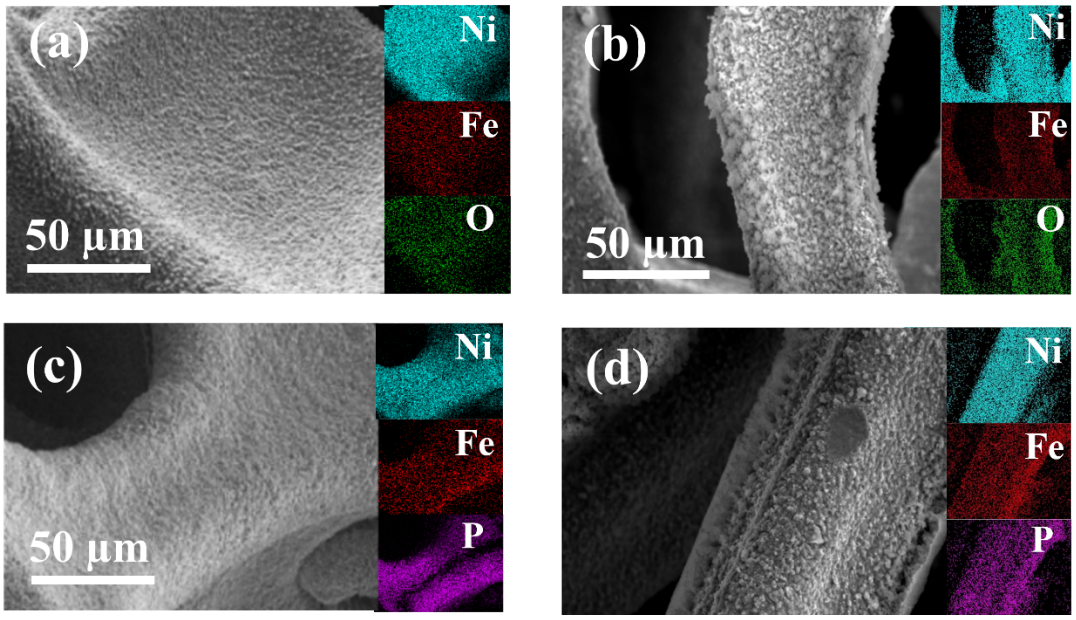

Figure S1 SEM images and surface element mappings of (a) NiFe foam, (b) o-NiFe foam, (c) NiFeP/NFF after 200 cycles of CV, and (d) o-NiFeP/NFF after 200 cycles of CV.

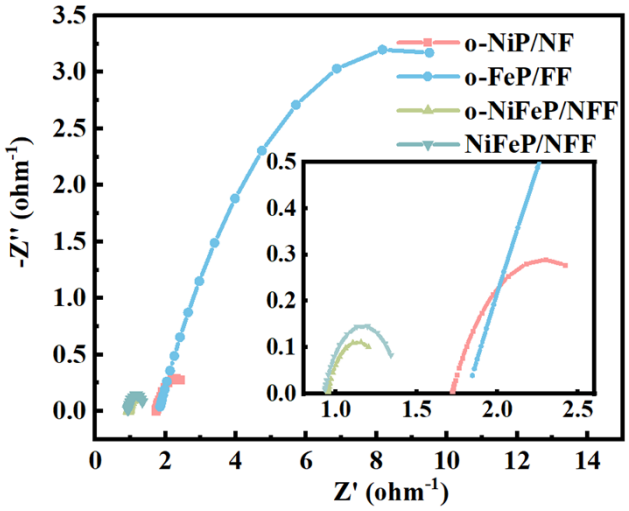

Figure S2. Nyquist plots of o-NiP/NF, o-FeP/FF, o-NiFeP/NFF, and NiFeP/NFF.

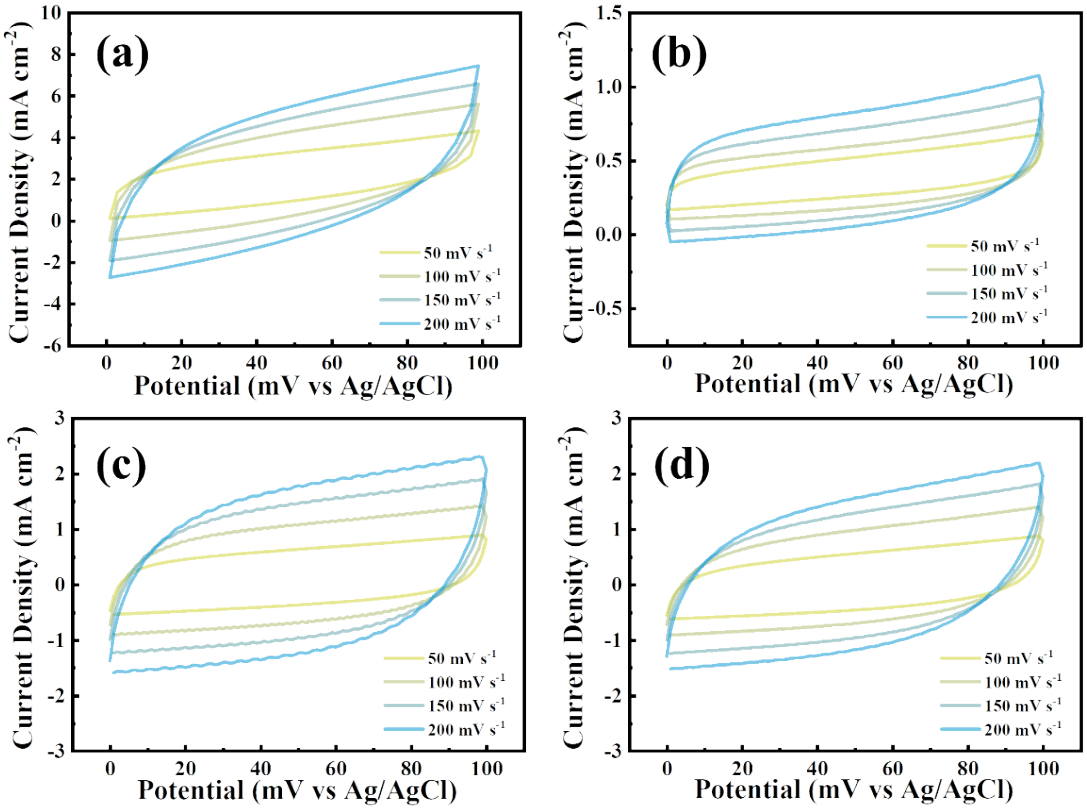

Figure S3. CV curves of (a) o-NiP/NF, (b) o-FeP/FF, (c) o-NiFeP/NFF, and (d) NiFeP/NFF samples obtained at 50, 100, 150 and 200 mV s^{-1} in the range of 0-100 mV vs. Ag/AgCl.

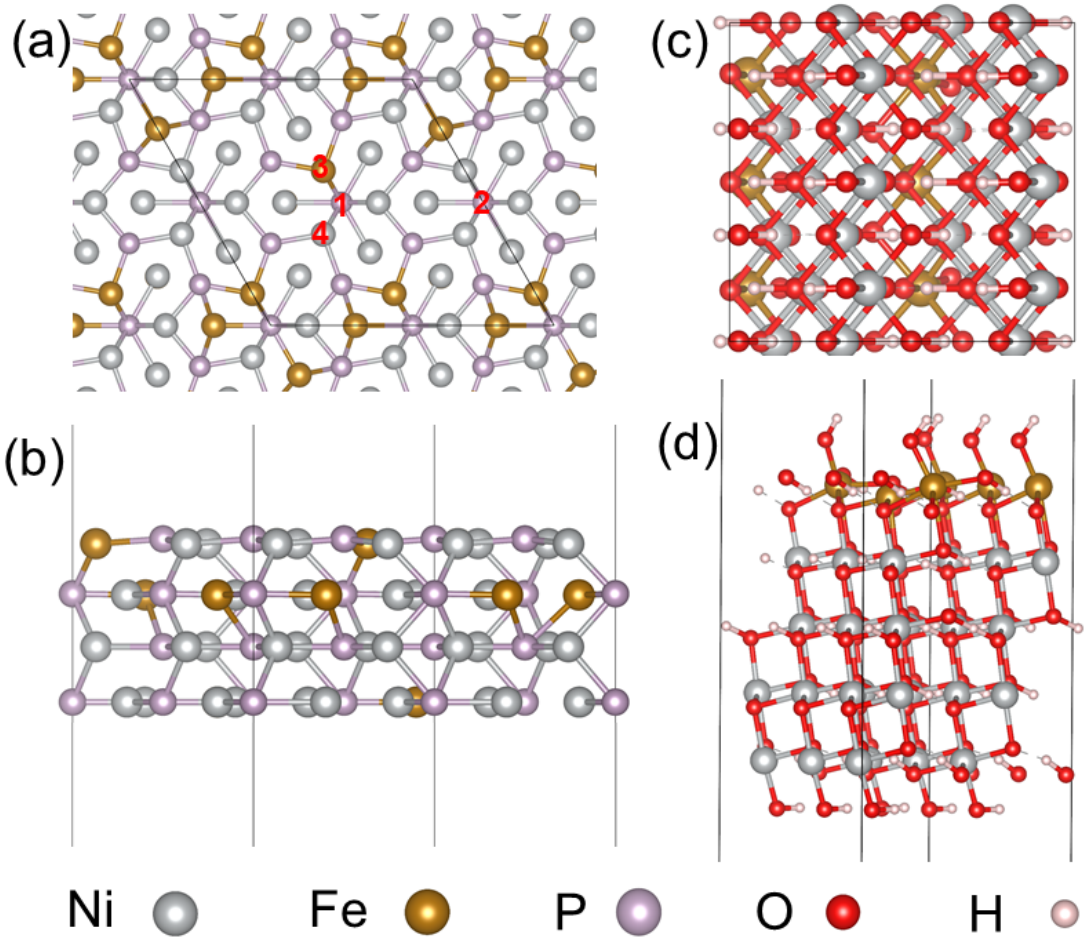

Figure S4. The top and front view of $Ni_{2-x}Fe_xP$ (a-b) and Fe(Ni)-rich upper (lower) surface of NiFeOOH (c-d). 1-4 mean the NiFe hollow site, Ni hollow site, Fe-top site and Ni-top site for OH adsorption.

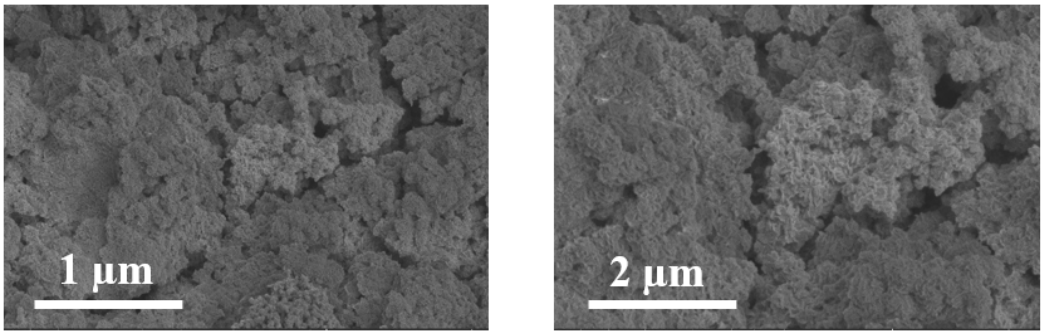

Figure S5. SEM images of o-NiFeP/NFF after being immersed in a 1.0 M potassium hydroxide solution

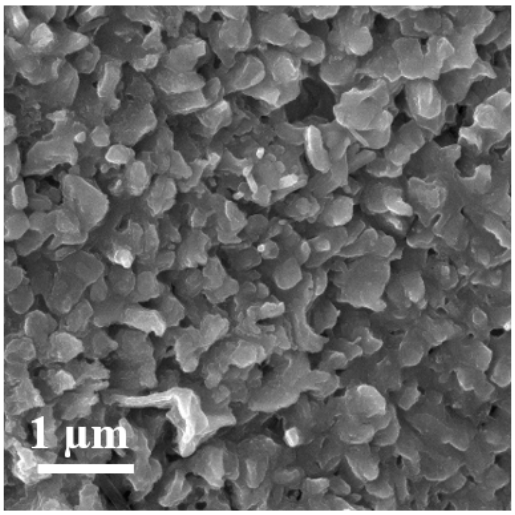

Figure S6. The SEM image of o-NiFeP/NFF after 468h testing

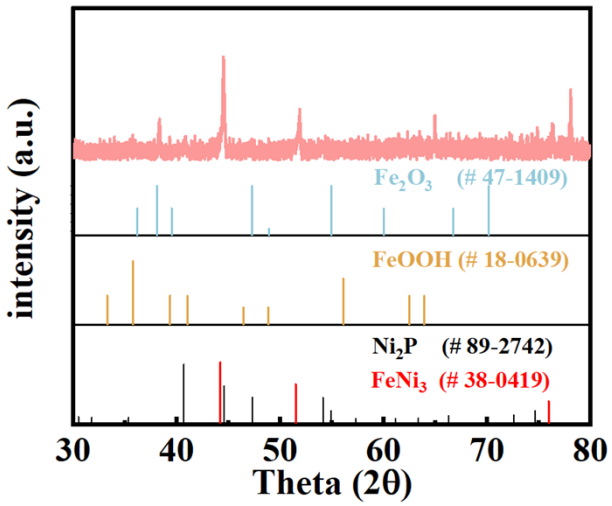

Figure S7. The XRD pattern of o-NiFeP/NFF after 468h testing.

Table S1 The generating mass of Ni^{2+}/Fe^{2+} along with the etching time when 1×1.5 cm^2 NiFe foam being soaked in 1.0 M HCl solutions by ICP-OES.

Dissolution time	m_{Fe} (mg)	m_{Ni} (mg)	$\Delta m_{Fe}/\Delta m_{Ni}$
t=10 min	0.99	0.11	9/1
t=20 min	1.80	0.20	9/1
t=30 min	2.43	0.27	9/1
All dissolved	23.78	19.91	1.20/1

Table S2 The elemental weight percentages measured from EDS.

Sample	Atomic Percentage (At%)				
	Ni	Fe	Fe/Ni+Fe	P	O
NiFe foam	96.14	3.13	0.032	-	0.71
o-NiFe foam	76.98	18.41	0.193	-	4.60
NiFeP/NFF	65.88	3.78	0.054	12.39	1.90
o-NiFeP/NFF	64.06	16.03	0.200	13.45	6.46
NiFeP/NFF after 200 cycles	71.97	3.68	0.048	13.09	11.25
o-NiFeP/NFF after 200 cycles	58.89	22.50	0.276	7.60	11.00

Table S3 Parameters obtained from the fitted plots using the relevant equivalent circuit.

Samples	R_{ct} (Ω)	CPE-T (F)	CPE-P (F)
o-NiP/NF	1.146	1.126	0.596
o-FeP/FF	13.69	0.023	0.558
o-NiFeP/NFF	0.369	1.625	0.694
NiFeP/NFF	0.479	0.554	0.699

Table S4 Tafel slope comparison of NiFe based oxides, layered double hydroxides, and phosphides for OER.

Samples	Electrolytes	Tafel slope (mV dec^{-1})	Ref.
$NiFe_2O_4$	1 M KOH	42	[9]
$NiFeO_x$/CFP	1 M KOH	32	[10]
α-$FeNiO_x$	0.1 M KOH	24	[11]
$NiFeO_x$ NTAs	1 M KOH	47	[12]
$Ni_{60}Fe_{40}O_x$	0.1 M KOH	34	[13]
O-NiFeLDH/NF	1 M KOH	29	[14]
NiFe-LDH	1 M KOH	40	[15]
FeNi-rGO LDH	1 M KOH	39	[16]
NiFeLDH-NS@DG/GCE	1 M KOH	52	[17]
Ni_2P/C@NF	1 M KOH	65	[18]
NiCoFeP	1 M KOH	83	[19]
NiFe-P/NF	1 M KOH	59	[20]
$(Ni_{0.5}Fe_{0.5})_2P$/NF	1 M KOH	57	[21]
$(Ni_{0.87}Fe_{0.13})_2P$/Ni	1 M KOH	96	[22]
Ni_2P/$(NiFe)_2P$(O)NA/NF	1 M KOH	60	[23]

Table S5 Calculated binding energy of OH on different sites of $Ni_{2-x}Fe_xP$.(eV)

Models	*NiFe-hollow*	Ni-hollow	Fe-top	Ni-top
Ni_2P	x	-3.93	x	-2.17
$Ni_{1.92}Fe_{0.08}P$	-4.27	-3.94	-3.17	-2.22
$Ni_{1.66}Fe_{0.33}P$	-4.29	-3.97	-3.20	-2.28

References

1. G. Kresse, J. Furthmüller, Efficient iterative schemes for ab initio total-energy calculations using a plane-wave basis set. *Phys. Rev. B* 1996, **54**, 11169.
2. G. Kresse, J. Furthmüller, Efficiency of ab-initio total energy calculations for metals and semiconductors using a plane-wave basis set. *Comput. mater. sci.* 1996, **6**, 15-50.
3. P. E. Blöchl, Projector augmented-wave method, *Physical review B*, 1994, **50**, 17953.
4. A. Petukhov, I. Mazin, L. Chioncel, A. Lichtenstein, Correlated metals and the LDA+ U method. *Phys. Rev.B* 2003, **67**, 153106.
5. S. Grimme, J. Antony, S. Ehrlich and H. Krieg, A consistent and accurate ab initio parametrization of density functional dispersion correction (DFT-D) for the 94 elements H-Pu, *The Journal of chemical physics*, 2010, **132**.
6. S. Grimme, S. Ehrlich and L. Goerigk, Effect of the damping function in dispersion corrected density functional theory, *Journal of computational chemistry*, 2011, **32**, 1456-1465.
7. J. K. Nørskov, T. Bligaard, A. Logadottir, J. Kitchin, J. G. Chen, S. Pandelov and U. Stimming, Trends in the exchange current for hydrogen evolution, *Journal of The Electrochemical Society*, 2005, **152**, J23.
8. J. K. Nørskov, J. Rossmeisl, A. Logadottir, L. Lindqvist, J. R. Kitchin, T. Bligaard and H. Jonsson, Origin of the overpotential for oxygen reduction at a fuel-cell cathode, *The Journal of Physical Chemistry B*, 2004, **108**, 17886-17892.
9. M. S. Al-Hoshan, J. P. Singh, A. M. Al-Mayouf, A. A. Al-Suhybani and M. N. Shaddad, Synthesis, Physicochemical and Electrochemical Properties of Nickel Ferrite Spinels Obtained by Hydrothermal Method for the Oxygen Evolution Reaction (OER), *Int J Electrochem Sc*, 2012, **7**, 4959-4973.
10. H. T. Wang, H. W. Lee, Y. Deng, Z. Y. Lu, P. C. Hsu, Y. Y. Liu, D. C. Lin and Y. Cui, Bifunctional non-noble metal oxide nanoparticle electrocatalysts through lithium-induced conversion for overall water splitting, *Nat Commun*, 2015, **6**.
11. R. D. L. Smith, M. S. Prevot, R. D. Fagan, Z. P. Zhang, P. A. Sedach, M. K. J. Siu, S. Trudel and C. P. Berlinguette, Photochemical Route for Accessing Amorphous Metal Oxide Materials for Water Oxidation Catalysis, *Science*, 2013, **340**, 60-63.
12. X. Teng, J. Y. Wang, L. L. Ji, Y. K. Lv and Z. F. Chen, Ni nanotube array-based electrodes by electrochemical alloying and de-alloying for efficient water splitting, *Nanoscale*, 2018, **10**, 9276-9285.
13. R. D. L. Smith, M. S. Prevot, R. D. Fagan, S. Trudel and C. P. Berlinguette, Water Oxidation Catalysis: Electrocatalytic Response to Metal Stoichiometry in Amorphous Metal Oxide Films Containing Iron, Cobalt, and Nickel, *J Am Chem Soc*, 2013, **135**, 11580-11586.
14. Z. Qiu, C. W. Tai, G. A. Niklasson and T. Edvinsson, Direct observation of active catalyst surface phases and the effect of dynamic self-optimization in

NiFe-layered double hydroxides for alkaline water splitting, *Energ Environ Sci*, 2019, **12**, 572-581.
15. F. Song and X. L. Hu, Exfoliation of layered double hydroxides for enhanced oxygen evolution catalysis, *Nat Commun*, 2014, **5**.
16. X. Long, J. K. Li, S. Xiao, K. Y. Yan, Z. L. Wang, H. N. Chen and S. H. Yang, A Strongly Coupled Graphene and FeNi Double Hydroxide Hybrid as an Excellent Electrocatalyst for the Oxygen Evolution Reaction, *Angew Chem Int Edit*, 2014, **53**, 7584-7588.
17. Y. Jia, L. Z. Zhang, G. P. Gao, H. Chen, B. Wang, J. Z. Zhou, M. T. Soo, M. Hong, X. C. Yan, G. R. Qian, J. Zou, A. J. Du and X. D. Yao, A Heterostructure Coupling of Exfoliated Ni-Fe Hydroxide Nanosheet and Defective Graphene as a Bifunctional Electrocatalyst for Overall Water Splitting, *Adv Mater*, 2017, **29**.
18. H. Q. Qu, Y. R. Ma, Z. L. Gou, B. Li, Y. R. Liu, Z. X. Zhang and L. Wang, Ni2P/C nanosheets derived from oriented growth Ni-MOF on nickel foam for enhanced electrocatalytic hydrogen evolution, *J Colloid Interf Sci*, 2020, **572**, 83-90.
19. K. H. Wang, Y. Y. Si, Z. H. Lv, T. P. Yu, X. Liu, G. X. Wang, G. W. Xie and L. H. Jiang, Efficient and stable Ni-Co-Fe-P nanosheet arrays on Ni foam for alkaline and neutral hydrogen evolution, *Int J Hydrogen Energ*, 2020, **45**, 2504-2512.
20. B. W. Zhang, Y. H. Lui, L. Zhou, X. H. Tang and S. Hu, An alkaline electro-activated Fe-Ni phosphide nanoparticle-stack array for high-performance oxygen evolution under alkaline and neutral conditions, *J Mater Chem A*, 2017, **5**, 13329-13335.
21. J. H. Yu, G. Z. Cheng and W. Luo, Hierarchical NiFeP microflowers directly grown on Ni foam for efficient electrocatalytic oxygen evolution, *J Mater Chem A*, 2017, **5**, 11229-11235.
22. J. H. Chen, Y. M. Li, G. Q. Sheng, L. Xu, H. Q. Ye, X. Z. Fu, R. Sun and C. P. Wong, Iron-Doped Nickel Phosphide Nanosheets InSitu Grown on Nickel Submicrowires as Efficient Electrocatalysts for Oxygen Evolution Reaction, *Chemcatchem*, 2018, **10**, 2248-2253.
23 W. G. Xi, G. Yan, Z. L. Lang, Y. Y. Ma, H. Q. Tan, H. T. Zhu, Y. H. Wang and Y. G. Li, Oxygen-Doped Nickel Iron Phosphide Nanocube Arrays Grown on Ni Foam for Oxygen Evolution Electrocatalysis, *Small*, 2018, **14**.